

Joint Pathology Center
Veterinary Pathology Services

WEDNESDAY SLIDE CONFERENCE
2020-2021

Conference 23

21 April, 2021



Joint Pathology Center
Silver Spring, Maryland

CASE 1: MS1401949 (JPC 4052879-00)

Signalment:

3 month old male C57BL/6N mouse

History:

A 3 month old male C57BL/6N mouse received total body irradiation of 900 rads and subsequently received 5×10^6 syngeneic bone marrow cells. Two months later the mouse was infected with 1.5×10^4 *Listeria monocytogenes* IV via tail vein injection. The mouse became morbid within days and was submitted for necropsy following euthanasia.

Gross Pathology:

The mouse was thin and contained a small amount of body fat. The spleen was of normal size but moderately pale and mottled. The liver was mildly enlarged uniformly. The heart, lungs, kidneys, GI tract, testes and brain appeared normal.

Laboratory results:

A sample of spleen was collected for bacterial culture and yielded a pure growth of *Listeria monocytogenes*.

Microscopic description:

Liver - There is multifocal, random acute coagulative necrosis throughout the section. Small numbers of degenerative neutrophils are

present along the margins of the necrotic foci. Intracellular bacilli are evident within hepatocytes at the margins of the necrotic foci. Mild to moderate intracellular lipodosis is present with the lipodosis being more prominent in hepatocytes at the margins of the necrotic foci.

Spleen - Multiple foci of necrosis are evident which appear to correspond primarily with lymphoid follicles. Degenerative neutrophils are evident adjacent to necrotic foci, within sinusoids and the capsule of the spleen. Short gram positive bacilli consistent with *Listeria monocytogenes* are evident within the spleen. Minimal extramedullary hematopoiesis is noted in the spleen.



Liver, spleen, mouse. A section of liver and spleen are submitted for examination. Multifocal to coalescing areas of pallor corresponding to necrosis are seen in both sections. (HE, 9X)

Lesions were not noted in other organs/tissues.

Contributor's morphologic diagnosis:

Spleen - splenitis, necrotizing, acute, severe

Liver - hepatitis, multifocal, necrotizing, acute, severe

Contributor's comment:

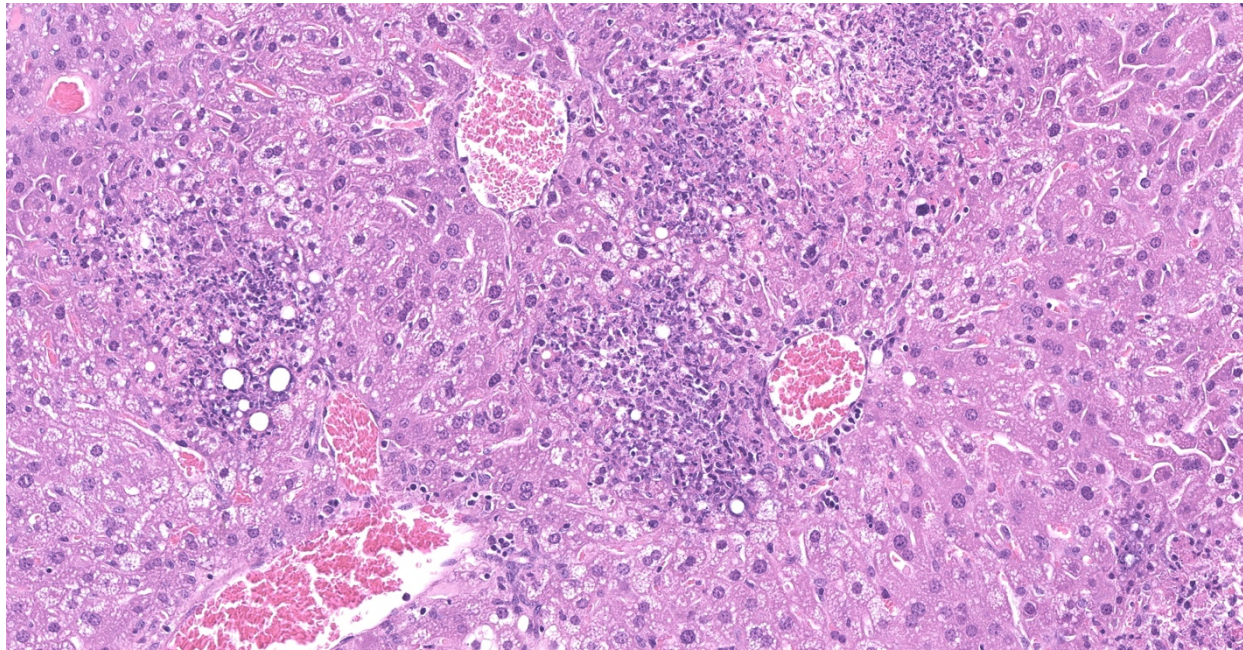
Listeria monocytogenes is a gram positive, facultative, intracellular bacillus. It is a ubiquitous agent found in the soil which can survive in the environment for months or longer. The agent is one of the leading causes of food-borne disease.

Listeria was first discovered by E.G.D. Murray in 1926 associated with outbreaks affecting rabbits and guinea pigs. The first human case was reported in 1929, with the first human epidemic associated with ingestion of contaminated food in 1983.² The organism grows best at -18° to 10° C. The ability to grow at these temperatures allows for transmission from foodstuffs which have been properly refrigerated. The agent has been isolated from raw and undercooked meat and poultry, processed meats, vegetables, soft cheeses, ice cream and unpasteurized milk. Vegetables can be

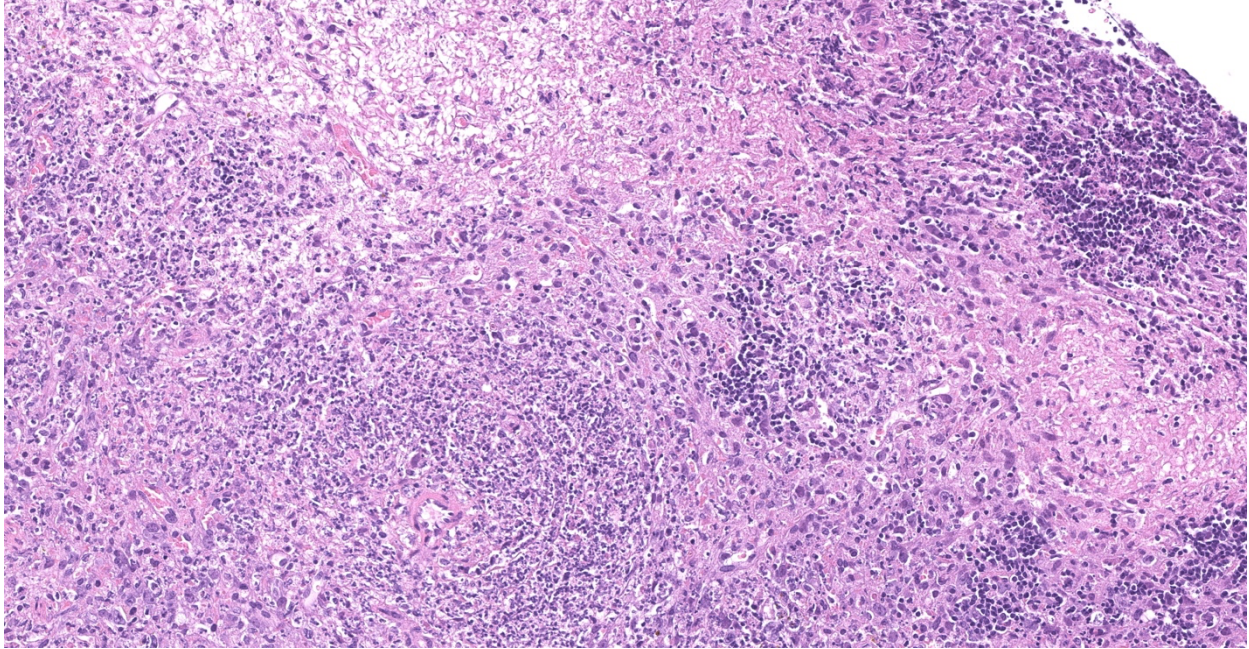
contaminated from soil or manure used as fertilizer.⁸

Human infections in the United States occur at approximately 2500 per year with a mortality rate of 20 to 30%. High risk groups include the elderly, infants, pregnant women, fetuses, and immunocompromised individuals. Infection of humans and animals is typically via ingestion of contaminated foodstuffs. The bacterium typically causes a self-limiting gastroenteritis and can reside in the intestinal tract for long periods without inducing disease.⁴

Infection beyond the gastrointestinal tract generally leads to one of three significant clinical syndromes - meningitis/meningoencephalitis, septicemia, and third trimester abortion. In humans, disease is typically manifested as a meningitis and/or meningoencephalitis. In animals listeriosis is primarily a disease of ruminants affecting sheep, cattle and goats and has also been reported in llamas, alpacas, deer, reindeer, antelope, water buffalo, moose and captive giraffe. Infection is often associated with ingestion of spoiled silage. The disease in ruminants is typically a CNS disorder with suppurative meningitis or meningoencephalitis



Liver, mouse. There are multifocal areas of lytic necrosis scattered randomly throughout the parenchyma, which begin as areas of coagulative necrosis which are then infiltrated by large numbers of neutrophils which become necrotic and add to the cellular debris. (HE, 212X)



Spleen, mouse. Coalescing areas of lytic necrosis efface both red and white pulp. (HE, 203X)

and cerebral microabscesses, with clinical signs including circling, ataxia, opisthotonos and possible cranial nerve paralysis. The CNS signs are due to centripetal migration along cranial nerves particularly the trigeminal nerve, with lesions commonly involving the brainstem, with gross evidence of meningitis along the ventral midbrain, pons and medulla oblongata. In ruminants, particularly sheep, infection may also be caused by *L. ivanovii*.⁶ In monogastric animals the disease is primarily a septicemia and has been reported in rodents and lagomorphs and rarely in dogs, cats, horse and swine. In nonhuman primates disease is rare and has been reported in chimpanzees, baboons, and Celebese black apes. Disease has also been reported in avian species including chickens, turkeys, ducks, geese, pigeons, canaries, parrots, eagles, owls and partridges.⁵ Mice are susceptible to experimental infection but are relatively resistant to infection orally and require administration by a parenteral route. Susceptibility to infection varies by strain with A/J and BALB/c being more sensitive to infection than C57BL/6.⁵

Infection follows invasion of the intestinal epithelium with replication in the lamina propria and extension to the mesenteric lymph nodes with dissemination to the liver and spleen. Secondary

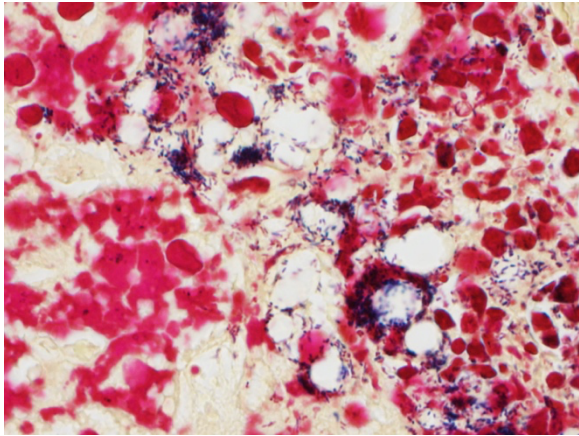
viremia can lead to dissemination to the cranial nerves and the meninges and to the placenta in pregnant females. Invasion of epithelial cells is receptor mediated and involves expression of internalin genes *inlA*, *inlB*, and *ami* on the surface of the bacterium which bind E-cadherin inducing adhesion. Following multiplication in the cytosol the bacteria induce actin polymerization to aid in direct transfer to adjacent cells. *Listeria monocytogenes* can enter dendritic cells and histiocytes via phagocytosis. Listeriolysin O, a secreted cholesterol induced cytolysin, mediates escape from the phagocytic vacuoles into the cytosol. Protection against the bacterium is mediated primarily by interferon gamma produced by NK and T cells.⁵

Contributing Institution:

National Institutes of Health
Division of Veterinary Resources
Diagnostic and Research Services Branch

JPC diagnosis:

1. Liver: Hepatitis, necrotizing, random, multifocal, marked, with numerous intracellular and extracellular bacilli.
2. Spleen: Splenitis, necrotizing, multifocal to coalescing, severe, with thrombosis and lymphocytolysis.



Liver, mouse. Numerous short gram-positive bacilli consistent with *Listeria monocytogenes* are concentrated at the perimeter of necrotic foci. (Brown-Brenn, 1000X)

JPC comment:

The contributor provides an excellent summary of *Listeria monocytogenes*. Because this bacterium causes significant disease in human populations, as well as animal populations, there is utility in tracking outbreaks and potentially drawing conclusions about patterns of infection. ProMED is an organization that aggregates official and unofficial data and provides resources and updates regarding disease outbreaks for a number of entities. Importantly, this data aggregation is publicly available, which can help inform the allocation of resources, evaluation of intervention efficacy, and novel aspects of the disease. A study of human *L. monocytogenes* cases from 1996-2018 covered the largest outbreak recorded, in South Africa, where there were more than 1000 laboratory confirmed cases, and more than 200 deaths. In the analyzed time period, there was also a marked increase in outbreaks involving novel foods not previously associated with *L. monocytogenes*. The increases are hypothesized to be due to changing food distribution methods and government regulation, the complexity of the global food distribution system, and the widespread consumption of ready to eat products.³

While to a great degree, *L. monocytogenes* is considered one entity, in reality, there are four evolutionary lineages, 13 serotypes, and four PCR groups within the species. Using multilocus

sequence typing (MLST), there are further subdivisions into clones. These distinctions come with varying pathogenicity, and variable expression of virulence factors. In addition to *InlA* (listeriolysin S cluster) and genes responsible for synthesis of teichoic acid, a collection of six genes that encode a cellobiose-family PTS system, which impacts sugar and carbon metabolism and confers increased neurovirulence and maternal-neonatal infection virulence. The collection of six genes has a proposed name of *Listeria* pathogenicity island 4 (LIPI-4). Other clones of *L. monocytogenes* lack LIPI-4, but are capable of causing disease, indicating that additional factors contributing to their virulence remain to be discovered.⁷

Investigation into extracellular vesicles secreted by Gram positive bacteria was neglected until recently, as it was erroneously considered unlikely given their thick peptidoglycan cell walls. However, biologically active extracellular vesicles have now been described for a variety of fungi and Gram positive bacteria, in addition to the previous body of knowledge for Gram negative bacteria. *L. monocytogenes* secretes vesicles 20-200 nm in diameter containing listeriolysin O and phosphatidylinositol-specific phospholipase C. When tested, cell-free preparations of extracellular vesicles were toxic to murine macrophage cells, helping *L. monocytogenes* to survive intracellularly within hosts. By packaging virulence factors in a vesicle, it allows for concentrated delivery, without dilution as a function of distance.¹

The moderator emphasized that while *L. monocytogenes* is relatively uncommon in mice, it is associated with abortion in rabbits. Other clinical manifestations include gastroenteritis, sepsis, and meningoencephalitis. As illustrated in this case, the experimental inoculation was performed as an intravenous injection, which has a higher degree of reproducibility in experimental models than oral infection.

References:

1. Coelho C, Brown L, Maryam M, et al. *Listeria monocytogenes* virulence factors, including listeriolysin O, are secreted in

- biologically active extracellular vesicles. *J. Biol. Chem.* 2019;294(4):1202-1217.
2. Cossart P. Listeriology (1926-2007): the rise of a model pathogen. *Microbes and Infection.* 2007; 9 (10): 1143-6.
 3. Desai AN, Anyoha A, Madoff LC, Lassmann B. Changing epidemiology of *Listeria monocytogenes* outbreaks, sporadic cases, and recalls globally: A review of ProMED reports from 1996 to 2018. *International Journal of Infectious Disease.* 2019;84:48-53.
 4. Lecuit, M. Human listeriosis and animal models. *Microbes and Infection.* 2007; 9: 1216-1225.
 5. D'Orazio S.E.F. Animal models for oral transmission of *Listeria monocytogenes*. *Front. Cell. Infect. Microbiol.* 2014; 11:4 15.
 6. Hoelzer K, Pouillot R and Dennis S. Animal models of listeriosis: a comparative review of the current state of the art and lessons learned. *Veterinary Research.* 2012; 43:18.
 7. Maury MM, Tsai YH, Charlier C, et al. Uncovering *Listeria monocytogenes* hypervirulence by harnessing its biodiversity. *Nat Genet.* 2016;48(3):308-313.
 8. Ramaswamy V, Cresence V, Rejitha, J, et al. *Listeria*-review of epidemiology and pathogenesis. *J Microbiol Immunol Infect.* 2007; 40:4-13.
-

CASE 2: 17-0367-2-3 (JPC 4101224-00)

Signalment:

Twelve-month-old, intact male Sprague-Dawley rat, *Rattus norvegicus*.

History:

The animal was part of a group of training rats; however, it had never been used for this purpose and was considered experimentally naïve. Health records indicated that the animal was reported clinically normal. During a recent regular check-up, a large ovoid mass was found slightly protruding from the right flank. The animal was euthanized and submitted for necropsy.

Gross Pathology:

The right kidney was completely effaced by a 3 cm x 2.5 cm, white to grayish, firm multinodular mass with multifocal areas of hemorrhages and

necrosis. A similar but smaller (1.2 cm in diameter) round white firm mass was also present on the caudal pole of the left kidney.

Laboratory results:

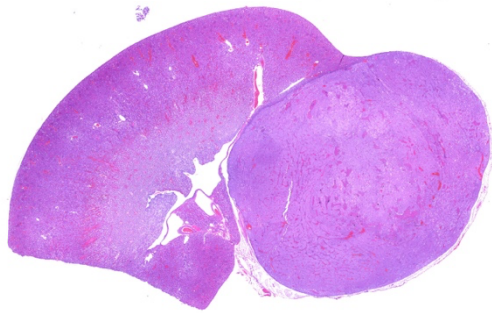
Not applicable.

Microscopic description:

Left kidney. Partially effacing the right kidney and compressing the adjacent normal parenchyma, there is a well demarcated, unencapsulated, expansile multinodular epithelial neoplasm characterized by a diffuse lobular pattern in which lobules are separated by thin bands of fibrovascular stroma. Lobules are composed of large, round to polygonal cells, with abundant amphophilic to eosinophilic cytoplasm. Neoplastic cells frequently display multiple small clear vacuoles within their cytoplasm or contain large clear intracytoplasmic vacuoles. Nuclei are round to oval with finely granular chromatin and 1 occasionally evident central magenta nucleolus. There is moderate cellular and nuclear pleomorphism with karyomegaly, and mitoses are rare. Scattered throughout the neoplasm, there are multifocal areas of coagulative necrosis within the center of the lobules, mineral deposition is seen. In the adjacent section of preserved kidney, tubules are occasionally dilated, lined by flattened tubular epithelial cells, and contain a moderate to abundant amount of eosinophilic homogeneous proteinaceous material. Occasional tubular basophilia is seen



Kidney, rat. The caudal pole of the kidney is effaced by a 1.4cm diameter pale white soft nodular mass. (Photo courtesy of: Laboratory of Comparative Pathology; Hospital for Special Surgery, Memorial Sloan Kettering Cancer Center, The Rockefeller University, Weill Cornell Medicine.)



Kidney, rat. Subgross magnification of the kidney and neoplasm at the caudal pole. (HE, 6X)

with mild thickening of the peritubular basement membrane. Small clusters of lymphocytes and plasma cells are rarely seen in the fibrovascular stroma adjacent to the neoplastic cells of within the preserved renal interstitium.

Contributor's morphologic diagnosis:

Kidneys: Amphophilic-vacuolar renal tubule carcinoma, bilateral.

Kidney, left: Mild multifocal tubular dilation with intraluminal hyaline casts and peritubular basophilia; minimal multifocal interstitial lymphoplasmacytic infiltrates.

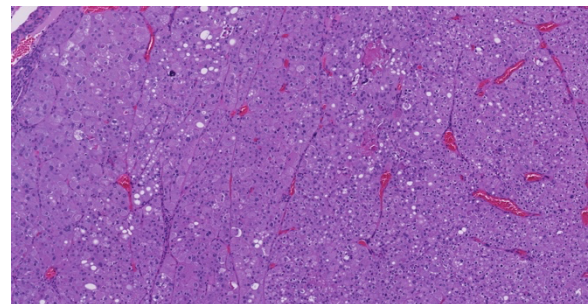
Contributor's comment:

Amphophilic-vacuolar (AV) tumors are a variant of renal tubule tumors (RTTs) exhibiting morphologic features that are different from the conventional RTTs.^{1,7,8,9} Specifically, AV tumors have a diffuse multilobular appearance in which lobules are separated by thin bands of fibrovascular stroma.¹ Lobules consist of tightly packed polygonal cells with distinct cell borders, abundant amphophilic to eosinophilic cytoplasm frequently containing numerous large clear vacuoles.^{1,9}

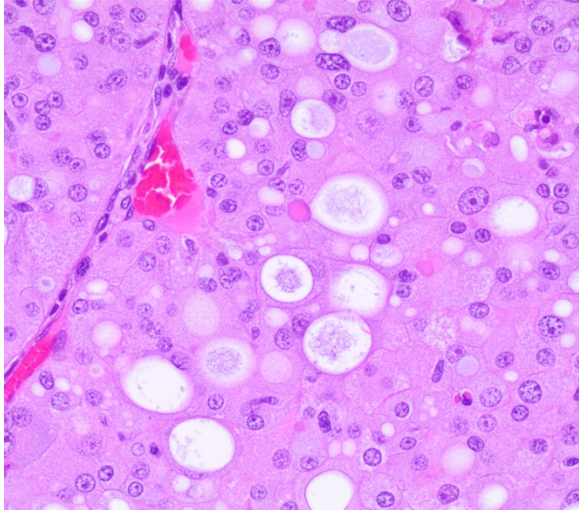
Tumors with AV phenotype can be seen in rats as part of the spectrum of hyperplasia, adenoma, and carcinoma identified for renal tumors.⁸ As reported in the present case, AV tumors are often multiple and/or bilateral.⁴ Furthermore, regions of atypical tubular hyperplasia characterized by more than a single cell layer forming a solid tubule or papillary projections can also be seen associated with it.^{1,5} The first report of spontaneous RTTs with AV features in rats

occurred nearly 60 years ago,² and it represented an example of a Mendelian inherited predisposition (autosomal dominant pattern) in which all heterozygous animals develop tumors).^{3,4} It is now known that its spontaneous occurrence in the Long-Evans (Eker) rat is due to mutations in the tuberous sclerosis gene (*Tsc2*).¹⁰ A tumor exhibiting similar morphologic features has also been observed in SD (Nihon) rats, and it is attributable to mutations in the Birt-Hogg-Dube' (*Bhd*) tumor suppressor gene.¹¹ Germline mutations in either of these 2 tumor suppressor genes predispose the rats to multicentric, bilateral renal tubular neoplasia and hyperplasia.⁶ In the Eker rat, tumors have a later onset and appear vacuolated and chromophilic; conversely, neoplasms in rats harboring the *Bhd* mutation exhibit an early onset and may have a clear cell, cystic, papillary, chromophobe, or eosinophilic appearance.¹¹

A previous report identified a low incidence of spontaneous AV tumors in one group of F344 littermates.¹⁶ AV tumors have been reported sporadically in several strains of young rats used in subchronic toxicity (90-days) studies,^{6,7,13} as well as in two-year carcinogenicity bioassays.⁸ Interestingly, they have been observed in control and treated groups,⁸ and have previously been demonstrated to be spontaneous, nontreatment-related.^{1,8,9} Additionally, their distinct histological profile clearly helped differentiating them from the conventional chemically induced RTTs.¹ Furthermore, in support of the familial nature of these neoplasms, it was not uncommon for multiple tumors to appear within the same toxicologic study where the animals are often littermates,¹ in the absence of underlying toxic/proliferative changes.⁶ Metastases of AV



Kidney, rat. Neoplastic cells are arranged in cords, and occasionally, smaller nests and packets. (HE, 103X)



Kidney, rat. Neoplastic cells often contain a large cytoplasmic vacuole with flocculent amphophilic debris. (Photo courtesy of: Laboratory of Comparative Pathology; Hospital for Special Surgery, Memorial Sloan Kettering Cancer Center, The Rockefeller University, Weill Cornell Medicine.)(HE, 200X)

tumors were not reported in the previous studies, at least in the lungs,⁸ and were not found in the present case. Complete blood count (CBC), serum chemistry and urinalysis were not performed prior to euthanasia. Minimal tubular ectasia accompanied by hyaline casts and multifocal tubular basophilia were noted histologically, and no other changes were found in the organs examined. These findings are compatible with an early stage of chronic progressive nephropathy (or CPN), which is one of the most common spontaneous lesions in rats and mice and it is commonly observed in nearly all male rats.⁵ Although no association with chronic progressive nephropathy was previously reported,⁸ the animal in the present case was older compared other animals diagnosed with AV tumors.^{1,6,11}

Given its aforementioned features, it has been proposed to record this distinctive renal tumor phenotype separately from conventional RTTs and allow for appropriate interpretation of the carcinogenic potential of a test article on the kidneys.^{1,8}

Contributing Institution:

Laboratory of Comparative Pathology; Hospital for Special Surgery, Memorial Sloan Kettering

Cancer Center, The Rockefeller University, Weill Cornell Medicine.

<https://www.mskcc.org/research-areas/programs-centers/comparative-medicine-pathology>

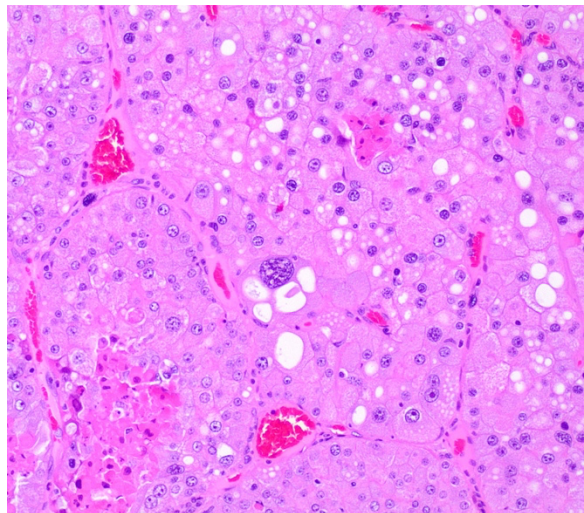
JPC diagnosis:

Kidney: Renal cell carcinoma, amphophilic-vacuolar type.

JPC comment:

The contributor provides a concise summary of this infrequently encountered renal tumor. A number of rats have been used as animal models of autosomal dominant gene associated renal tumors, including the Eker and Nihon rats. Others, such as Sprague-Dawley, Fischer 344, and Wistar rats also experience spontaneous proliferative renal lesions. As of this writing, there have been no reports of metastasis, or chemical induction of these tumors.¹⁵

In rats, basophilic carcinomas with well organized lobules are the most common carcinomas. While clear cell and papillary carcinomas occur in the rat, they are much less frequent, and anaplastic and sarcomatoid variants are rare. For purposes of classification, both amphophilic vacuolar type neoplasms and



Kidney, rat. Occasional karyomegalic cells are scattered throughout the neoplasm, and nests of neoplastic cells often demonstrate areas of central necrosis (lower left). (Photo courtesy of: Laboratory of Comparative Pathology; Hospital for Special Surgery, Memorial Sloan Kettering Cancer Center, The Rockefeller University, Weill Cornell Medicine.)(HE, 200X)

oncocytomas should be considered distinct and separate from basophilic tumor types.⁵

A recent report of three cases of AV tumors in Sprague-Dawley rats participating in a 2-year carcinogenicity study highlight the scientific gaps in our knowledge of this disease pathogenesis and progression. The animals were all in placebo control groups, and so contribute to the evidence for familial disease in these rats.¹²

A number of histologically similar neoplasms have recently been reported in Tg.Rash2 mice in 26-week carcinogenicity studies. The lesions were adenomas and a carcinoma with amphophilic staining of polygonal cells, and tumors demonstrated cystic and/or papillary patterns. Because these lesions are thought to be familial in rats, a trace back to the parents of affected mice was performed. However, there was no correlation in lesions between generations. The lesions in affected mice all presented with multiple neoplasms, either multiple foci in one kidney, or lesions in both kidneys. These likely arose as spontaneous lesions.¹⁴

References:

1. Crabbs TA, Frame SR, Laast VA, Patrick DJ, Thomas J, Zimmerman B, Hardisty JF. Occurrence of spontaneous amphophilic-vacuolar renal tubule tumors in Sprague-Dawley rats from subchronic toxicity studies *Toxicol Pathol* 2013; 41: 866-871.
 2. Eker R. Familial renal adenomas in Wistar rats—A preliminary report. *Acta Pathol Microbiol Scand* 1954; 34: 554–562.
 3. Eker R and Mossige J. A dominant gene for the renal adenomas in the rat. *Nature* 1961; 189: 858-859.
 4. Everitt JI, Goldsworthy TL, Wolf DC, Walker CL. Hereditary renal cell carcinoma in the Eker rat: A rodent familial cancer syndrome. *J Urol* 1992; 148: 1932–1936.
 5. Frazier KS, Seely JC, Hard GC, Betton G, Burnett R, Nakatsuji S, Nishikawa A, Durchfeld-Meyer B, Bube A. Proliferative and nonproliferative lesions of the rat and mouse urinary system. *Toxicol Pathol* 2012; 40: 14S-86S.
 6. Hall WC, Elder B, Walker CL, Cai S, Peters DG, Goodman DG, Ulland BM, Borzelleca JF. Spontaneous renal tubular hyperplastic and neoplastic lesions in three Sprague Dawley rats from a 90-day toxicity study. *Toxicol Pathol* 2007; 35: 233–241.
 7. Hard GC, Long PH, Crissman JW, Everitt JI, Yano BL, Bertram TA. Atypical tubule hyperplasia and renal tubule tumors in conventional rats on 90- day toxicity studies. *Toxicol Pathol* 1994; 22:489–496.
 8. Hard GC, Seely JC, Kissling GE, Betz LJ. Spontaneous occurrence of a distinctive renal tubule tumor phenotype in rat carcinogenicity studies conducted by the National Toxicology Program. *Toxicol Pathol* 2008; 36: 388–396.
 9. Hardisty JF, Banas DA, Gopinath C, Hall WC, Hard GC, Takahashi M. Spontaneous renal tumors in two rats from a thirteen week rodent feeding study with grain from molecular stacked trait lepidopteran and coleopteran resistant (DP-004114-3) maize. *Food Chem Toxicol* 2013; 53: 428-431.
 10. Kobayashi T, Hirayama Y, Kobayashi E, Kubo Y, Hino O. A germline insertion in the tuberous sclerosis (Tsc2) gene gives rise to the Eker rat model of dominantly inherited cancer. *Nat Gen* 1995; 9: 70–74.
 11. Kouchi M, Okimoto K, Matsumoto I, Tanaka K., Yasuba M, Hino O. Natural history of the Nihon (Bhd gene mutant) rat, a novel model for human Birt-Hogg-Dube' syndrome. *Virchows Arch* 2006; 448: 463–471.
 12. Kudo K, Hoshiya T, Nakazawa T, et al. Spontaneous renal tumors suspected of being familial in Sprague-Dawley rats. *J Toxicol Pathol*. 2012;25:277-280.
 13. Lanzoni A, Pialia A, Everitt J, Faustinelli I, DeFazio R, Cavaliere L, Cristofori P. Early onset of spontaneous renal preneoplastic and neoplastic lesions in young conventional rats in toxicity studies. *Toxicol Pathol* 2007; 35: 589–593.
 14. Paranjpe MG, Belich JL, McKeon ME, et al. Renal tumors in 26-week Tg.Rash2 mice carcinogenicity studies. *Toxicol Pathol*. 2016;44(5):633-635.
 15. Seely JC, Hard GC, Blankenship B. Kidney. In: Suttie AW, ed. *Boorman's Pathology of the Rat*. San Diego, CA:Elsevier. 2018:147-149.
 16. Thurman JD, Hailey JR, Turturro A, Gaylor DW. Spontaneous renal tubular carcinoma in Fischer-344 rat littermates. *Vet Pathol* 1995; 32: 419–422.
-

CASE 3: 2019 Case 1 (JPC 4135948-00)

Signalment:

4.7 months old male Dunkin-Hartley guinea pig (*Cavia porcellus*)

History:

This guinea pig boar was obtained from the supplier with a jugular vein catheter and enrolled in an infectious disease imaging study. Following baseline imaging and bloodwork, this animal was experimentally infected followed by imaging and elective euthanasia on post-infection day 3.

Gross Pathology:

N/A

Laboratory results:

	Baseline	Terminal	RI
WBC	6.25	4.47	3.12-8.71
Neutrophil	2560	3490	932-3935
Lymphocyte	3320	790	771-5058
Monocyte	260	170	128-629
Platelets	536	251	155-545
Hematocrit	45.2	44.0	34.3-56.1
Glucose	165	214	129-215
Creatinine	0.4	0.7	0.2-0.7
BUN	18	14	11-21
Calcium	10.8	10.7	9.5-11.6
Albumin	2.7	2.5	1.9-3.3
Total Protein	4.7	4.7	4.0-5.8
ALP	93	88	79-259
TBili	0.3	0.3	0.2-0.4
GGT	16	9	5-31
Amylase	1093	1090	861-1613

Microscopic description:

Slide contains sections of serous (parotid), mucinous (sublingual) and mixed (submandibular) salivary glands as well as thymus, cervical lymph nodes, thyroid, and skeletal muscle. Unilaterally affecting the parotid and sublingual glands there is focally extensive central coagulative necrosis and edema. At the margins of the lesions, with variable ingress to the center and replacement of infarcted tissues, there is florid infiltrate of densely cellular plump spindle cells (fibroblasts) with scant nascent edematous stroma, frequent macrophages and few neutrophils. Embedded within this process are numerous intralobular ducts, the morphology of which ranges from normal to crowded and

stratified with cytoplasmic basophilia and frequent mitotic figures. There is scattered squamous metaplasia of the ducts with prominent desmosomes in the stratum spinosum. Some ducts within areas of coagulative necrosis are lined by attenuated basophilic cells with necrotic cell debris in the center. Acute fibrin thrombi or fragments of re-endothelialized and organized thrombus are visible in some small arteries, with plump hypertrophied endothelium lining the intima. Edema and nascent fibroplasia circumscribe both glands.

Contributor's morphologic diagnosis:

Parotid and sublingual salivary glands, unilateral, coagulative necrosis (infarct), focally extensive, subacute to chronic, severe with fibroplasia and ductal hyperplasia and squamous metaplasia

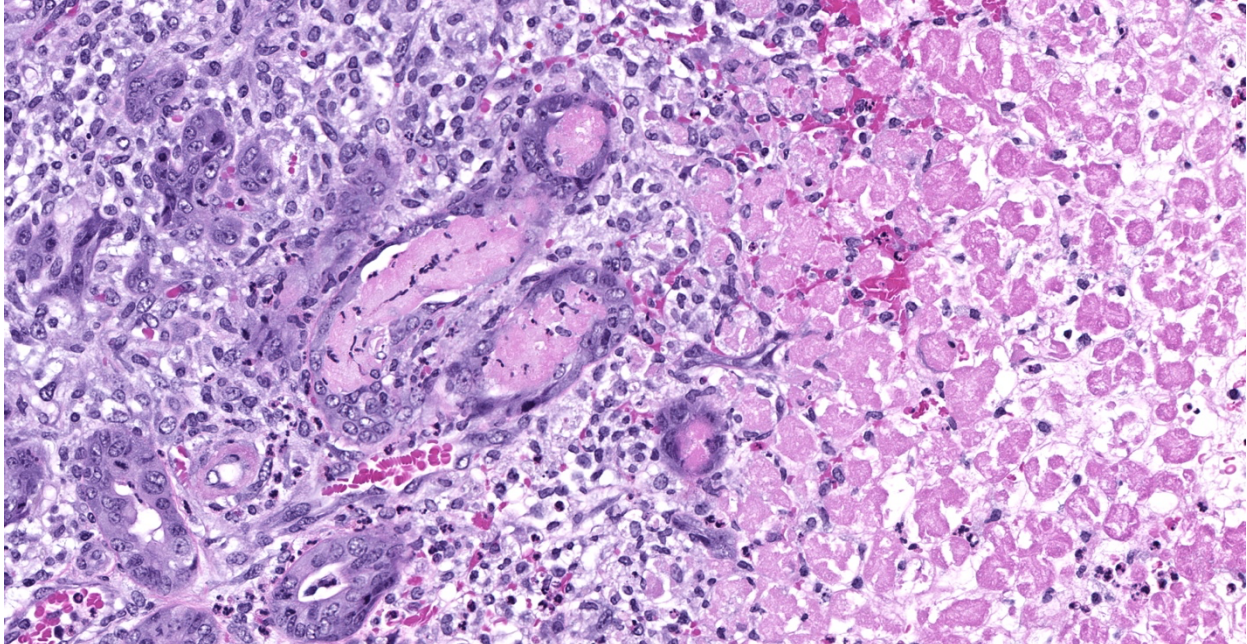
Contributor's comment:

Necrotizing sialometaplasia is a rare, poorly understood reactive lesion presumed to follow ischemic damage to the salivary gland. It has been previously reported in dogs, cats, and a laboratory rabbit.^{1,3,8,12} In humans, the lesion often affects the minor salivary glands of the palate, but can uncommonly affect major salivary glands.^{2,5} In addition to presenting as a mass lesion, dogs may have clinical signs including ptyalism, dysphagia and vomiting.⁴ It is important not to misdiagnose the process as squamous cell carcinoma with desmoplasia, particularly with cytology or small biopsy samples.

This guinea pig was obtained from the supplier at approximately 2 months of age with a catheter



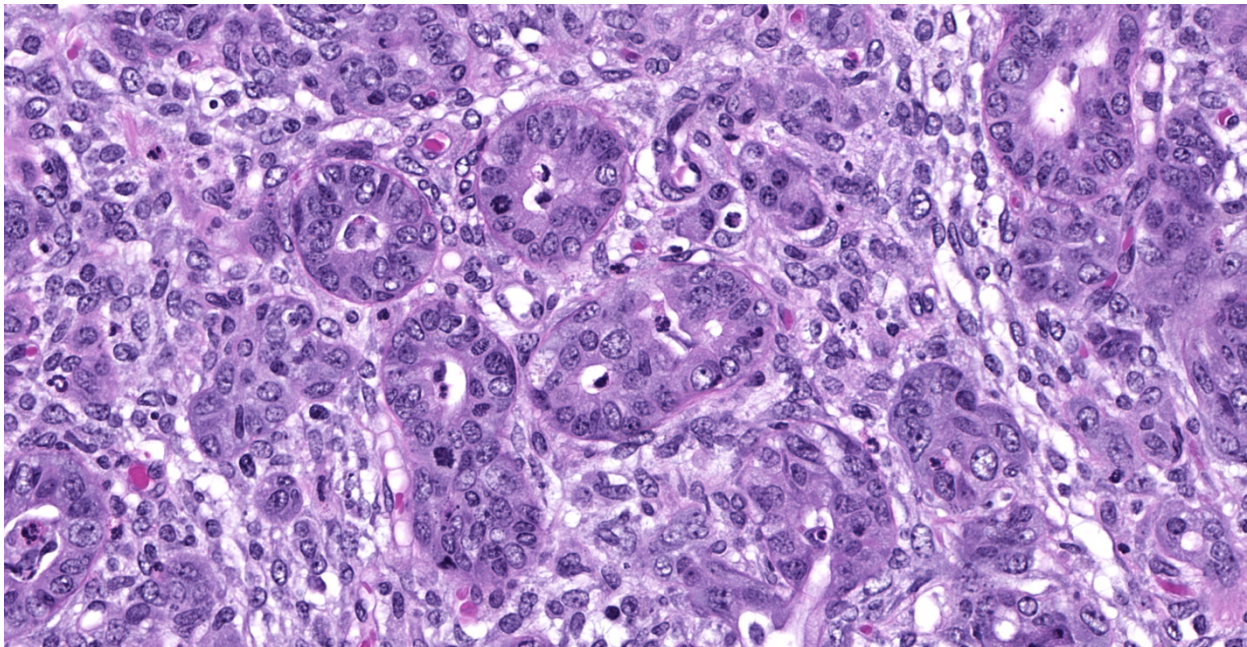
Multiple organs, guinea pig. Sections of parotid salivary gland, thyroid, cervical lymph node, submandibular and sublingual salivary gland, and thymus are presented for examination. At left, there is a large area of pallor within the submandibular gland and stain affinity is poor in multiple lobes of the salivary gland. (HE, 5X)



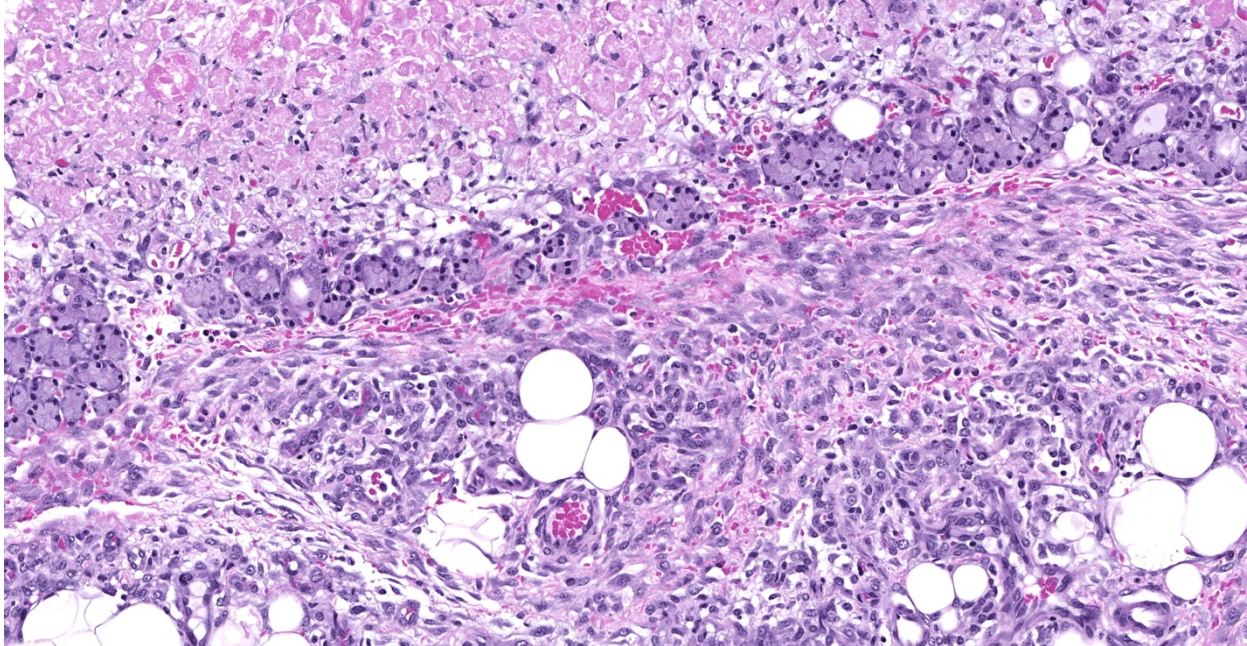
Submandibular salivary gland, guinea pig. Higher magnification of the periphery of the infarct. Salivary gland undergoing coagulative necrosis is at right. At the periphery, ducts demonstrate regenerative changes including deep basophilia, large nuclei, and mitotic figures. Ductal lumina contain brightly eosinophilic debris. There is disorganization of acini at left, with shrunken and disorganized acinar cells with poor delineation of cellular borders and lack a lumen (atrophy). Moderate numbers of neutrophils expand the interstitium. (HE, 260X)

implanted in the right jugular vein. This procedure includes a percutaneous stay suture near the junction of the jugular vein and cranial vena cava. In this case, it is suspected that the suture may have inadvertently ligated the arterial supply to the ipsilateral parotid and sublingual

salivary glands, resulting in infarction. The guinea pig salivary glands receive blood from the superficial cervical artery, maxillary artery, lingual artery, and cranial laryngeal artery.¹⁰ Based on location of the stay suture, it is likely that the superficial cervical artery was affected.



Submandibular salivary gland, guinea pig. In other areas of the gland, there is ductal proliferation with numerous mitotic figures. (HE, 393)



Submandibular salivary gland, guinea pig. At the periphery of the infarct which border the interlobular septa, there is infiltration of the periglandular fat and effacement of glandular tissue by granulation tissue and inflammation. (HE, 169X)

The lesion was considered incidental and unrelated to experimental manipulations. It should be recalled that in guinea pigs the thymus is located in the cranioventral neck rather than the mediastinum.⁶

Contributing Institution:

Pathology Department

NIH/NIAID

Integrated Research Facility

<https://www.niaid.nih.gov/about/integrated-research-facility>

JPC diagnosis:

Salivary gland, submandibular: Coagulative necrosis (infarct), multifocal, with ductular degeneration, necrosis, and regeneration, squamous metaplasia, and acinar atrophy.

JPC comment:

In a recent analysis of 179 canine salivary lesions in Georgia (United States), approximately 2.2% of lesions were necrotizing sialometaplasia, with approximately half of cases diagnosed as non-specific sialoadenitis. Similar to this case, described cases of necrotizing sialometaplasia were characterized by extensive areas of coagulative necrosis bordered by mixed

inflammation and fibrosis, vascular thrombosis, and duct hyperplasia with squamous metaplasia.⁷

Cases of necrotizing sialometaplasia have been reported in other species as well. Previous reports have indicated 5-13% of feline salivary lesions involve infarction, leading to necrotizing sialometaplasia. However, while human cases usually involve known causes of vascular damage or ischemia, a cause has not been identified in cats.¹

In a study comparing the efficacy of different therapies for reducing the volume of the inferior nasal turbinate tissue in pigs, the 6 week post potassium titanyl phosphate (KTP) laser treatment patients had remarkable necrotizing sialometaplasia in the lamina propria, with cystic glands and excess mucous production. The KTP laser emits light at 532 nm, readily absorbed by hemoglobin, and causes endothelial impairment and thrombosis. The resulting coagulative necrosis is typically confined to a depth of 0.5 mm, with subsequent necrotizing sialometaplasia found in this region.¹¹

The moderator and conference participants discussed the diagnostic criteria for this entity, which includes 1) massive infarction, 2) bland

nuclear features, 3) squamous metaplasia of the ducts and acini, 4) inflammation and granulation tissue, and 5) maintenance of the glandular lobular structures. This entity may be misdiagnosed as mucoepidermoid, squamous cell carcinoma, or subacute necrotizing sialoadenitis.^{9,12}

References:

1. Brown PJ, Bradshaw JM, Sozmen M, Campbell RH: Feline necrotising sialometaplasia: a report of two cases. *J Feline Med Surg* 2004;6(4):279-281.
2. Carlson DL: Necrotizing sialometaplasia: a practical approach to the diagnosis. *Arch Pathol Lab Med* 2009;133(5):692-698.
3. Kelly DF, Lucke VM, Denny HR, Lane JG: Histology of salivary gland infarction in the dog. *Vet Pathol* 1979;16(4):438-443.
4. Kelly DF, Lucke VM, Lane JG, Denny HR, Longstaff JA: Salivary gland necrosis in dogs. *Vet Rec* 1979;104(12):268.
5. Kim YH, Joo YH, Oh JH: A case of necrotizing sialometaplasia involving bilateral parotid glands. *Am J Otolaryngol* 2013;34(2):163-165.
6. Klapper CE: The development of the pharynx of the guinea pig with special emphasis on the morphogenesis of the thymus. *Am J Anat* 1946;78:139-180.
7. Lieske DE, Rissi DR. A retrospective study of salivary gland diseases in 179 dogs (2010-2018). *J Vet Diag Invest.* 2020;32(4):604-610.
8. Mukaratirwa S, Petterino C, Bradley A: Spontaneous necrotizing sialometaplasia of the submandibular salivary gland in a Beagle dog. *J Toxicol Pathol* 2015;28(3):177-180.
9. Shin SA, Na HY, Choe JY, et al. Necrotizing sialometaplasia: a malignant masquerade but questionable precancerous lesion, report of four cases. *BMC Oral Health.* 2020;20:206.
10. Shively MJ, Stump JE: The systemic arterial pattern of the guinea pig: the head, thorax, and thoracic limb. *Am J Anat* 1974;139(2):269-284.
11. Somogyari K, Moricz P, Gerlinger I, et al. Morphological and histological effects of radiofrequency and laser (KTP and Nd:YAG) treatment of the inferior turbinates in animals: A comparative pilot study. *Surgical Innovation.* 2016;24(1):5-14.
12. Villano JS, Cooper TK: Mandibular fracture and necrotizing sialometaplasia in a rabbit. *Comp Med* 2013;63(1):67-70.

CASE 4: 2020-WSC2 (JPC 4157768-00)

Signalment:

8 week old, female, Syrian hamster

History:

This Syrian hamster was on study for validation of a SARS-CoV-2 animal model. This animal was immunosuppressed through pretreatments with Cyclophosphamide. Although weight loss was noted clinically, the animal demonstrated signs of recovery and was euthanized thirteen days following challenge.

Gross Pathology:

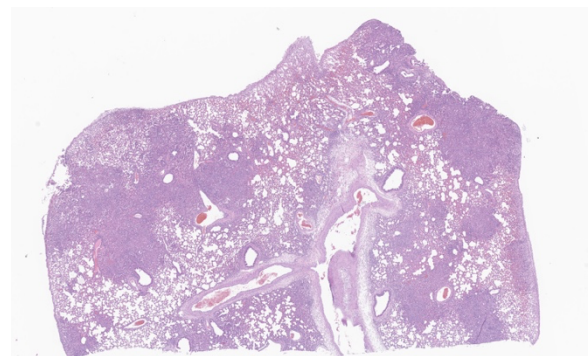
At necropsy, lung lobes were speckled red with minimal amounts of fluid in the pleural cavity.

Laboratory results:

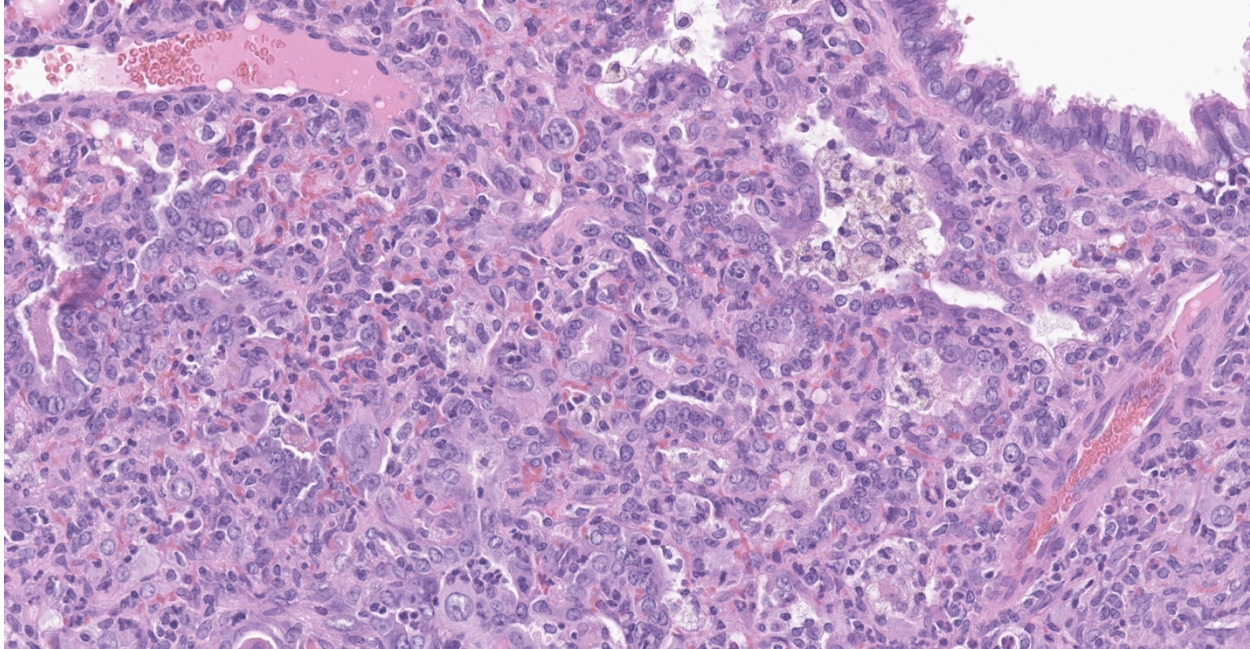
N/A

Microscopic description:

Lung: Affecting greater than 60% of the pulmonary parenchyma at all levels are multifocal to coalescing, random, and patchy areas of consolidation admixed with dense aggregates of macrophages, heterophils, fewer lymphocytes, multinucleate cells, necrotic cellular debris, hemorrhage, fibrin, and edema. Alveolar lumina contain swollen alveolar



Lung, hamster. There is multifocal to coalescing areas of pulmonary consolidation. The outpouching of the bronchial wall seen at low magnification is a function of cut. (HE, 5X)



Lung, hamster: Higher magnification of the inflammation in consolidated areas with diffuse filling of alveolar spaces and airways with exudate, interstitial expansion and marked hyperplasia of Type II pneumocytes and bronchiolar epithelium. (HE, 310X)

macrophages, previously mentioned inflammatory cells, hemorrhage, and necrotic debris. Within areas of consolidation alveolar septa are lined by palisading segments of low cuboidal epithelium (type II pneumocyte hyperplasia). Alveolar septa in these areas are expanded by inflammatory cells, fibrin, hemorrhage, and edema (septal necrosis). Inflammatory cells expand the peribronchial and peribronchiolar connective tissue with increased clear space (edema). Bronchial and bronchiolar epithelial cells exhibit the following: hyperplasia characterized by being bunched, stacked, and layered up to 4 cell layers thick, degeneration characterized by swelling, vacuolation and variable loss of cilia, and necrosis characterized by shrinking with a scant amount of hypereosinophilic cytoplasm and a pyknotic nucleus. The pleura is diffusely expanded up to 4x normal thickness by fibrous connective tissue, macrophages, heterophils, and lymphocytes. The pleural surface is lined by plump, reactive mesothelium (hypertrophy).

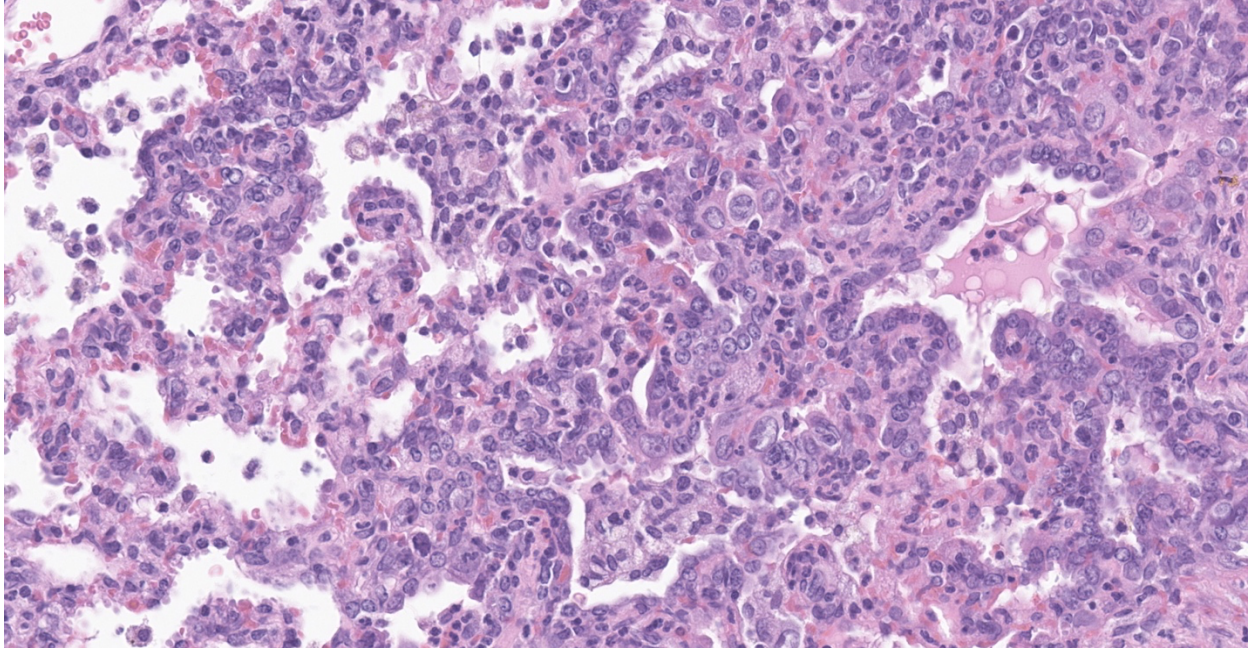
Contributor's morphologic diagnosis:

Lung: Pneumonia, bronchiointerstitial, necrotizing, histiocytic, heterophilic, multifocal, marked with type II pneumocyte hyperplasia, hamster (*Mesocricetus auratus*), rodent.

Contributor's comment:

Coronaviruses are enveloped RNA viruses that can lead to intestinal and respiratory infections in humans and animals.^{8,15} A novel coronavirus infection identified as Coronavirus Disease 2019 (COVID-19) can result in severe and fatal pneumonia which was identified in patients from Wuhan City, Hubei Province, China in December 2019.¹⁹ The subsequent pandemic and dearth of knowledge regarding this emerging pathogen resulted in widespread research efforts to further characterize the pathogen, disease course, and potential animal models.

Attachment and entry of SARS-CoV-2 is mediated by the human angiotensin-converting enzyme 2 (ACE2) receptor which is expressed primarily in lung (airway epithelial cells and type II pneumocytes), intestine, kidney, and heart.^{7,18} Expression of ACE2 mRNA has also been described in the brain, testis, liver, spleen, bone marrow, thymus, lymph nodes, skin, and mucosa of the oral and nasal cavity.³ Histologic features of the disease in humans reflect that of SARS-CoV to include diffuse alveolar damage (DAD), hyaline membrane formation with multinucleate viral syncytial cells, and pulmonary edema.¹⁶



Lung, hamster. In consolidated areas, alveolar septa are markedly expanded by macrophages, circulating neutrophils, edema, and marked Type II pneumocyte hyperplasia, many of which have markedly enlarged nuclei. In addition, there is hyperplasia of small bronchiolar epithelium, which extends into adjacent alveoli. This particular area is at the periphery of an area of consolidation in order to allow for better visualization of individual cellular components. (HE, 380X)

Since identification of the novel coronavirus, a number of studies have been conducted to establish an animal model to further characterize the disease and support therapeutic development efforts. At present, animal models include hamsters^{2,14}, non-human primates^{11,12,17}, ferrets^{4,13} and mice.¹ In the present study, the most notable histologic lesions at 13 days post-challenge (dpc) were identified in nasal turbinates and lungs. There is olfactory mucosal erosion and/or ulceration with multifocal, olfactory epithelial necrosis that can be overlaid by a pseudomembrane of necrotic debris and degenerate inflammatory cells. Additional findings include moderate to marked submucosal edema and infiltration by heterophils and lymphocytes. The predominant finding in lungs were diffuse, bronchial to bronchiolar epithelial hyperplasia with a patchy, mosaic of pulmonary consolidation. Areas of consolidation contained dense aggregates of macrophages, heterophils, necrotic debris, type II pneumocyte hyperplasia, and multinucleate cells. Reported histopathologic lesions from hamsters infected with SARS-CoV-2 at earlier stages of infection include epithelial cell degeneration of the trachea, diffuse alveolar damage and hyaline membrane formation in the

lungs, and congestion of nasal turbinate submucosa.²

Although not clearly identified for SARS-CoV-2, multinucleate cells have been observed in SARS-CoV infection. Based on immunoreactivity with CD68, multinucleate cells have been identified as macrophage origin.⁶ The susceptibility of ferrets and cats are considered high, with dogs being of low susceptibility and pigs, chicken, and ducks being not susceptible.¹² Reports of companion animal infection by SARS-CoV-2 have been reported, but data regarding post-mortem and microscopic findings in these species are limited. The significance of these findings in the context of zoonotic spread has yet to be determined and warrants further study.

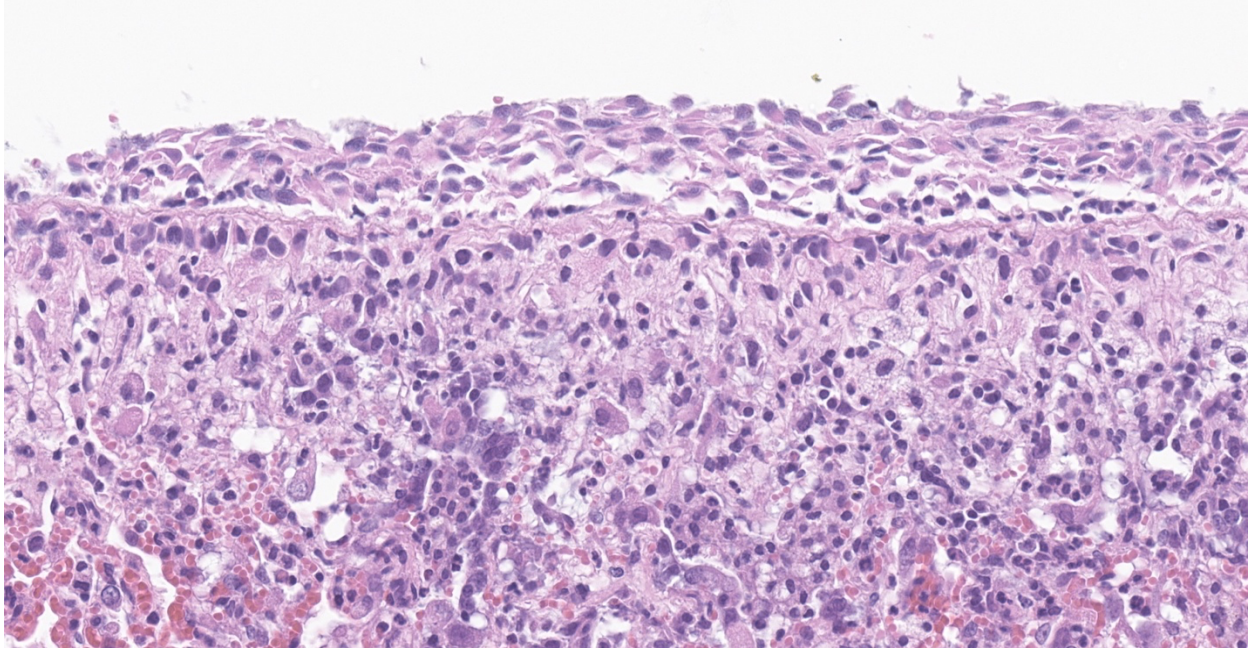
Contributing Institution:

USAMRIID

<https://www.usamriid.army.mil/>

JPC diagnosis:

Lung: Pneumonia, bronchiointerstitial, neutrophilic and histiocytic, multifocal to coalescing, subacute, severe, with marked Type II pneumocyte hyperplasia with syncytia formation, and multifocal septal necrosis.



Lung, hamster. There are aggregates of foamy macrophages in subpleural alveoli, and the pleura is segmentally covered with hyperplasia mesothelium. (HE, 380X)

JPC comment:

The contributor provides a concise summary on this case of SARS-CoV-2 in a hamster. A number of models of SARS-CoV-2 have been investigated, but serious natural disease has been experienced in mink farms.

The mink farming industry has recently received renewed attention due to the SARS coronavirus-2 (COVID-19) that has caused a worldwide pandemic and high rates of morbidity and mortality in human populations. Europe currently has an estimated 2750 mink farms, producing in excess of 27 million pelts annually. Due to the density of minks in group housing, transmissible disease often has ample opportunity to spread through farms. In early 2020, respiratory disease was noted in a number of mink farms in Denmark, which was isolated and confirmed to be SARS-CoV-2. In November 2020, the Ministry of Environment and Food of Denmark announced the culling of all mink in the country, due to concerns surrounding virus mutation. A number of coronaviral spike mutations had been noted in virus isolated from mink, leading to less effective neutralization by antibodies in a subset of humans that had been infected.^{5,10}

SARS-CoV-2 has a similar presentation in mink as humans. Mink examined in the Netherlands had experienced respiratory disease, and an increase in mortality. Clinical signs also included watery to mucoid nasal exudates and anorexia as the disease progressed. Affected animals had grossly apparent interstitial pneumonia characterized by all lobes swollen, dark red, and did not collapse. Histologically, lungs had diffuse alveolar damage, type II pneumocyte hyperplasia, thickening of alveolar septa by fibrillar eosinophilic material and mononuclear cells, with alveolar exudate consisting of desquamated cells, mononuclear inflammatory cells, and low numbers of neutrophils. Bronchiolar epithelial cells were characterized by severe necrosis with syncytial cells. Pulmonary alveolar edema with abundant foamy alveolar macrophages, perivascular edema, and hyperemia of alveolar septa were also consistent findings. Immunohistochemistry demonstrated strong immunolabeling for SARS-CoV-2 in epithelial cells of the bronchi and bronchioles, alveolar epithelial cells, and desquamated pneumocytes and macrophages.⁹

References:

1. Bao L, Deng W, Huang B, et al. The pathogenicity of SARS-CoV-2 in hACE2

- transgenic mice [published online ahead of print, 2020 May 7]. *Nature*. 2020.
2. Chan JF, Zhang AJ, Yuan S, et al. Simulation of the clinical and pathological manifestations of Coronavirus Disease 2019 (COVID-19) in golden Syrian hamster model: implications for disease pathogenesis and transmissibility [published online ahead of print, 2020 Mar 26]. *Clin Infect Dis*. 2020
 3. Jin Y, Yang H, Ji W, et al. Virology, Epidemiology, Pathogenesis, and Control of COVID-19. *Viruses*. 2020;12(4):372. Published 2020 Mar 27.
 4. Kim YI, Kim SG, Kim SM, et al. Infection and Rapid Transmission of SARS-CoV-2 in Ferrets. *Cell Host Microbe*. 2020;27(5):704-709.e2.
 5. Koopmans M. SARS-CoV-2 and the human-animal interface: outbreaks on mink farms. *Lancet Infect Dis*. 2021; 21(1):18-19.
 6. Kuiken T, Fouchier RA, Schutten M, et al. Newly discovered coronavirus as the primary cause of severe acute respiratory syndrome. *Lancet*. 2003;362(9380):263-270.
 7. Lu R, Zhao X, Li J, et al. Genomic characterisation and epidemiology of 2019 novel coronavirus: implications for virus origins and receptor binding. *Lancet*. 2020;395(10224):565-574.
 8. Masters, PS, and Perlman S. (2013) Coronaviridae. In *Fields Virology*. pp. 825-858.
 9. Molenaar RJ, Vreman S, Honing RWHD, et al. Clinical and Pathological Findings in SARS-CoC-2 Disease Outbreaks in Farmed Mink (*Neovison vison*). *Vet Path*. 2020; 57(5):653-657.
 10. Munnink BBO, Sikkema RS, Nieuwenhuije DF, et al. Transmission of SARS-CoV-2 on mink farms between humans and mink and back to humans. *Science*. 2021; 371(6525):172-177.
 11. Munster VJ, Feldmann F, Williamson BN, et al. Respiratory disease in rhesus macaques inoculated with SARS-CoV-2 [published online ahead of print, 2020 May 12]. *Nature*. 2020.
 12. Rockx B, Kuiken T, Herfst S, et al. Comparative pathogenesis of COVID-19, MERS, and SARS in a nonhuman primate model. *Science*. 2020;368(6494):1012-1015.
 13. Shi J, Wen Z, Zhong G, et al. Susceptibility of ferrets, cats, dogs, and other domesticated animals to SARS-coronavirus 2. *Science*. 2020;368(6494):1016-1020.
 14. Sia SF, Yan LM, Chin AWH, et al. Pathogenesis and transmission of SARS-CoV-2 in golden hamsters [published online ahead of print, 2020 May 14]. *Nature*. 2020;10.1038
 15. Weiss SR, Leibowitz JL. Coronavirus pathogenesis. *Adv Virus Res* 2011;81:85-164.
 16. Xu Z, Shi L, Wang Y, et al. Pathological findings of COVID-19 associated with acute respiratory distress syndrome [published correction appears in *Lancet Respir Med*. 2020 Feb 25;:]. *Lancet Respir Med*. 2020;8(4):420-422.
 17. Yu P, Qi F, Xu Y, et al. Age-related rhesus macaque models of COVID-19. *Animal Model Exp Med*. 2020;3(1):93-97.
 18. Zemlin AE, Wiese OJ. Coronavirus disease 2019 (COVID-19) and the renin-angiotensin system: A closer look at angiotensin-converting enzyme 2 (ACE2) [published online ahead of print, 2020 Jun 2]. *Ann Clin Biochem*. 2020.
 19. Zhu N, Zhang D, Wang W, et al. A Novel Coronavirus from Patients with Pneumonia in China, 2019. *N Engl J Med*. 2020;382(8):727-733.